Eur. Phys. J. A **9**, 439–451 (2000)

THE EUROPEAN PHYSICAL JOURNAL A

Shell model structures in the N = 46 isotones ^{86}Zr, ^{87}Nb, ^{88}Mo, ^{89}Tc, ^{90}Ru and ^{91}Rh

E. Galindo, A. Jungclaus, and K.P. Lieb[a]

II. Physikalisches Institut, Universität Göttingen, Bunsenstr. 7-9, D-37073 Göttingen, Germany

Received: 31 July 2000 / Revised version: 18 December 2000
Communicated by D. Schwalm

Abstract. The known level energies, electromagnetic moments and decay probabilities of high-spin states in the $N = 46$ isotones ^{86}Zr, ^{87}Nb, ^{88}Mo, ^{89}Tc, and ^{90}Ru are interpreted within the shell model. The single-particle space was truncated to the $p_{1/2}$ and $g_{9/2}$ orbits (relative to the ^{88}Sr core) and the single-particle energies and empirical two-body matrix elements derived by Gross and Frenkel were used in the calculations. Based on the generally good success of this approach, energies and decay properties of the yrast spectra in ^{90}Ru and ^{91}Rh are predicted.

PACS. 21.60.Cs Shell model – 23.20.Lv Gamma transitions and level energies – 21.10.-k Properties of nuclei

1 Introduction

Nuclei near the $N = 50$ neutron shell closure were among the first to which the nuclear shell model was applied in the early days of nuclear spectroscopy [1,2]. The rather good $Z = 38$ proton shell closure and the pronounced $N = 50$ neutron shell closure single out the $p_{1/2}$ and $g_{9/2}$ single-particle orbits as being active, and, indeed, many facets of $N = 48$–50 nuclei have been explained within this very truncated model space. This includes, *e.g.*, the nature of isomeric states (as a consequence of the large spin difference between the two orbits) and of the ground and first excited 0^+ state in ^{90}Zr. For the $N = 48$ and 49 isotones, the empirical shell model parameters deduced by Gross and Frenkel [3] have been particularly successful in describing energies and decay properties of high-spin states in the $38 \leq Z \leq 43$ nuclei which have been measured via heavy-ion fusion reactions, over the last two decades [4]. A similar conclusion was drawn by Herndl and Brown [5], who used the parametrisation of Gloeckner and Serduke [2] and calculated binding energies and β-decay halflives near the proton drip line as input for astrophysical processes. For the more neutron-deficient $N = 46$ isotones, a wealth of new spectroscopic information has been gathered via in-beam γ-ray spectroscopy at various $4\pi\gamma$-ray spectrometers, including lifetimes and magnetic moments [6–16]. Moreover, information on the neutron excitation across the $N = 50$ shell gap in the $N = 48$–50 isotones became available and decays of these states to the $(p_{1/2}, g_{9/2})$ states were identified, *e.g.*, in ^{93}Tc, ^{94}Ru and ^{95}Rh [17–21]

Table 1. Largest components of the GF-1 wave functions of high-spin states in ^{86}Zr (π means $\pi(g_{9/2})$ and ν means $\nu(g_{9/2})$).

E_x(keV)	$I^\pi(\hbar)$	Wave function	Fraction (%)
3299	8^+	ν_8^{-2}	87
4327	10^+	ν_{10}^{-4}	62
		$\pi_2^2 \otimes \nu_8^{-2}$	22
5397	12^+	$\pi_8^2 \otimes \nu_4^{-2}$	18
		ν_{12}^{-4}	16
		$\pi_4^2 \otimes \nu_8^{-2}$	13
		$\pi_6^2 \otimes \nu_6^{-2}$	13
6322	14^+	$\pi_8^2 \otimes \nu_6^{-2}$	58
		$\pi_6^2 \otimes \nu_8^{-2}$	28
		$\pi_8^2 \otimes \nu_8^{-2}$	8
7016	15^+	$\pi_8^2 \otimes \nu_8^{-2}$	81
		$\pi_8^2 \otimes \nu_7^{-4}$	9
7397	16^+	$\pi_8^2 \otimes \nu_8^{-2}$	88
		$\pi_6^2 \otimes \nu_{10}^{-4}$	7
8249	17^+	$\pi_8^2 \otimes \nu_{10}^{-4}$	60
		$\pi_8^2 \otimes \nu_9^{-4}$	23
		$\pi_6^2 \otimes \nu_{12}^{-4}$	9
8650	18^+	$\pi_8^2 \otimes \nu_{10}^{-4}$	83
		$\pi_6^2 \otimes \nu_{12}^{-4}$	9
		$\pi_8^2 \otimes \nu_{12}^{-4}$	7
9892	19^+	$\pi_8^2 \otimes \nu_{12}^{-4}$	100
10143	20^+	$\pi_8^2 \otimes \nu_{12}^{-4}$	100

The evolution from the "spherical" region, described by multiparticle shell model configurations, and the "deformed" region, characterized by strong $E2$ transitions and rotational band structures, appears to occur near neu-

[a] e-mail: lieb@physik2.uni-goettingen.de

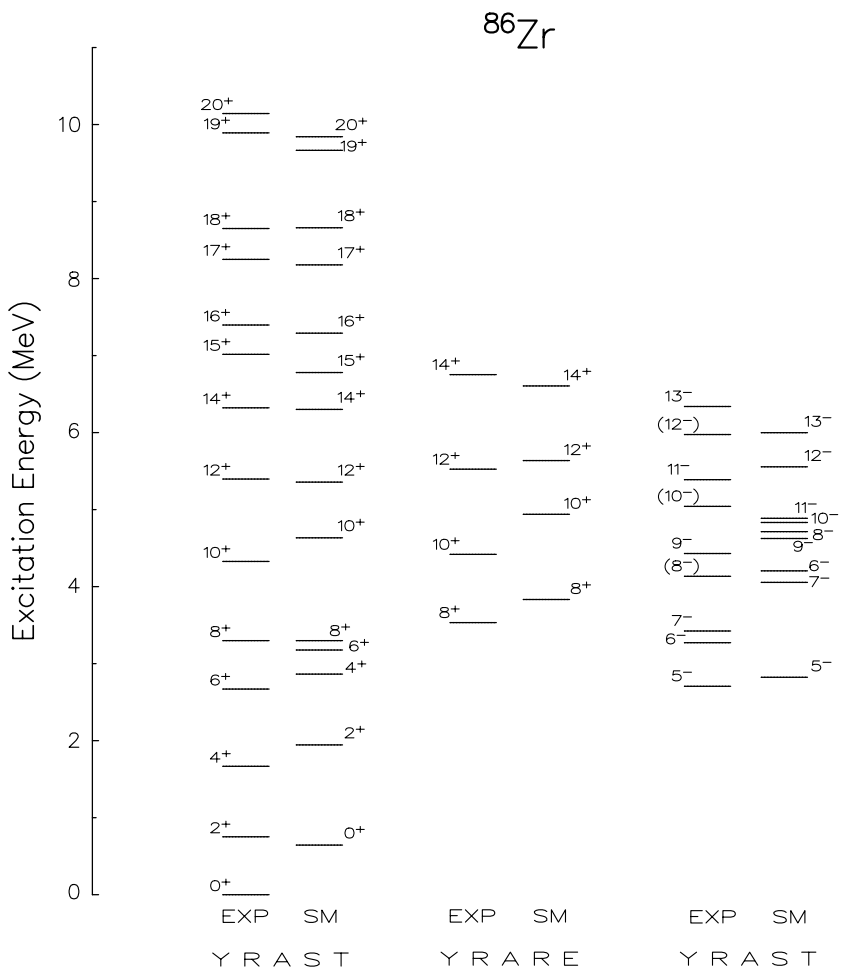

Fig. 1. Experimental [6,7] and calculated level scheme of ^{86}Zr

tron number $N = 46$ [8,22,23]. According to the calculated ground-state deformations [23] and the systematics of the even-A Mo isotopes [24], this transition develops rather suddenly as function of the neutron number. The experimentally observed variations of $E2$ strengths along the yrast lines in ^{87}Mo ($N = 45$) and ^{87}Nb ($N = 46$) indicate sudden changes of the deformation as function of the spin (and the number of aligned particles) [8,22]. In order to account for these aspects in ^{84}Zr and ^{86}Zr, the Yale group [7] used a hybride model which accomodates the collective quadrupole degree of freedom via the Interacting Boson Model [25] and the single-particle aspects by explicitly considering two or four $g_{9/2}$ valence nucleons above the first backbend.

The present systematic extension of the Gross-Frenkel shell model calculations to the $N = 46$ isotones with proton number $40 \leq Z \leq 45$ was motivated by
i) the wealth of recent experimental information on these nuclei, including level energies, magnetic moments and lifetimes of yrast and yrare states;
ii) the obvious success of the shell model for $N \geq 47$ nuclei and some difficulties of the IBM-2qp approach in ^{86}Zr (see below);
iii) the wish to identify quantities which are particularly sensitive to the model description and thus in future experiments may serve to find out in which direction the present simple approach has to be extended, in particular when pushing the spectroscopy towards ^{100}Sn;
iv) the extension to high-spin states which are outside the chosen single-particle space. Such states may arise either from proton excitations out of the $(p_{3/2}, f_{5/2})$ orbits or from neutron and/or proton excitations across the $N = 50$ shell gap, *i.e.* from the $g_{9/2}$ into the $d_{5/2}$ orbit. Such neutron excitations have recently been discussed in the $N = 50$ isotones ^{94}Ru and ^{95}Rh, on the basis of magnetic moments and highly retarded $M1$ and $E2$ transitions [19–21].

In section 2 we will briefly discuss the basic quantities and parameters of the Gross-Frenkel shell model calculations [3]. Detailed results for the high-spin states in the $N = 46$, $Z = 40$–45 isotones within the $(p_{1/2}, g_{9/2})$ space will be presented in section 3. General conclusions concerning the quality of the calculations and possible extensions will be summarized in section 4.

Table 2. Calculated and experimental branching ratios in ^{86}Zr.

E_x (keV)	I_i^π	E_γ (keV)	I_f^π	b(%) Exp	b(%) GF-1	E_x (keV)	I_i^π	E_γ (keV)	I_f^π	b(%) Exp	b(%) GF-1
						8650	18_1^+	401	17_1^+	52(5)	83
Positive Parity								1254	16_1^+	48(5)	17
3533	8_2^+	234	8_1^+	86(2)	86	9892	19_1^+	1242	18_1^+	37(13)	92
		863	6_1^+	14(1)	14			1643	17_1^+	63(13)	8
4327	10_1^+	1028	8_1^+	100	99	10143	20_1^+	251	19_1^+	16(4)	45
		794	8_2^+	n.o.	1			1493	18_1^+	84(4)	55
4419	10_2^+	92	10_1^+	n.o.	15						
		886	8_2^+	$\leq$55	85	*Negative Parity*					
		1120	8_1^+	$\geq$45	0	3424	7_1^-	151	6_1^-	n.o.	47
5397	12_1^+	1070	10_1^+	72(1)	81			718	5_1^-	100	53
		978	10_2^+	28(1)	19	4134	8_1^-	710	7_1^-	19(2)	97
6322	14_1^+	925	12_1^+	100	91			862	6_1^-	81(2)	3
		797	12_2^+	n.o.	9	4430	9_1^-	296	8_1^-	n.o.	15
7016	15_1^+	694	14_1^+	100	59			1006	7_1^-	100	85
		263	14_2^+	n.o.	41	5389	11_1^-	347	10_1^-	n.o.	84
7397	16_1^+	381	15_1^+	73(4)	91			959	9_1^-	100	16
		644	14_2^+	n.o.	0	5975	12_1^-	586	11_1^-	n.o.	100
		1075	14_1^+	26(4)	9			933	10_1^-	100	0
8249	17_1^+	852	16_1^+	67(9)	69	6339	13_1^-	364	12_1^-	n.o.	96
		1233	15_1^+	33(9)	31			950	11_1^-	100	4

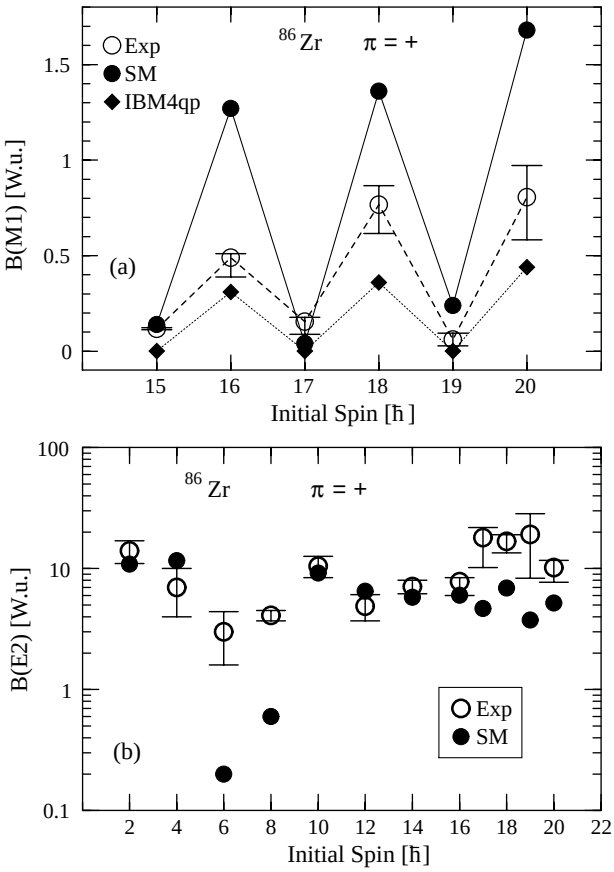

Fig. 2. Experimental [6,7] and calculated $M1$ (a) and $E2$ (b) transition strengths in ^{86}Zr.

2 Details of the calculations

All calculations were performed with the Utrecht shell model program RITSSCHIL developed by Zwarts [26]. The configuration space was restricted to the $(p_{1/2}, g_{9/2})$ proton and neutron orbits, using the single-particle energies and effective two-body matrix elements derived by Gross and Frenkel [3]. The effective single-particle charges and magnetic moments were taken from the $E2$ transition strengths and magnetic dipole moments in the $N = 49$ and 48 isotopes: $e_\pi = 1.72e$, $e_\nu = 1.44e$, $g_\pi(g_{9/2}) = +1.38$, $g_\nu(g_{9/2}) = -0.24$, $g_\pi(p_{1/2}) = -0.28$, and $g_\nu(p_{1/2}) = +1.26$. These parameters were used in all our previous calculations in this mass region [4]. The possible dependence of the effective charges on the valence orbit, discussed, *e.g.*, by Johnstone and Towner [27], was neglected. Further details of the calculations are given in [4], where the present parametrization was labeled GF-1.

In the even-even nuclei ^{86}Zr, ^{88}Mo, and ^{90}Ru, the experimental and theoretical level schemes were lined up in energy at the $I^\pi = 8^+$ yrast states, and in the odd-A isotones ^{87}Nb and ^{89}Tc at the $I^\pi = 21/2^+$ yrast states. At least near $Z = 40$, these states should have a rather pure $\pi^v(g_{9/2})$ partition, *i.e.* seniority $v = 2$ for even A and $v = 3$ for odd A, according to their measured magnetic moments [28,29]. The mean level deviations (MLD-1) quoted below refer to this normalization. When comparing experimental and theoretical $M1$ transition strengths, we assumed experimentally pure magnetic dipole transitions in the case of stretched $\Delta I = 1$ transitions, whenever no mixing ratio δ was known. For calculating theoretical branching ratios, we used the experimental transition energies.

Table 3. Main partitions of the calculated wave functions in ^{87}Nb. ($\bar{\pi} = \pi(p_{1/2})$, $\pi = \pi(g_{9/2})$, $\bar{\nu} = \nu(p_{1/2})$ and $\nu = \nu(g_{9/2})$).

E_x(keV)	I^π	Wave function		Fraction (%)
Positive Parity				
267	$7/2^+$	$\pi^3_{7/2}$		50
		$\pi^1_{9/2}$	ν^{-2}_2	24
		$\pi^3_{7/2}$	ν^{-2}_2	15
4	$9/2^+$	$\pi^1_{9/2}$		74
		$\pi^1_{9/2}$	ν^{-2}_2	14
1051	$11/2^+$	$\pi^1_{9/2}$	ν^{-2}_2	65
		$\pi^1_{9/2}$	ν^{-2}_4	21
785	$13/2^+$	$\pi^1_{9/2}$	ν^{-2}_2	66
		$\pi^1_{9/2}$	ν^{-2}_4	13
1954	$15/2^+$	$\pi^1_{9/2}$	ν^{-2}_6	47
		$\pi^1_{9/2}$	ν^{-2}_4	30
1737	$17/2^+$	$\pi^1_{9/2}$	ν^{-2}_4	70
		$\pi^1_{9/2}$	ν^{-2}_6	10
2491	$21/2^+$	$\pi^1_{9/2}$	ν^{-2}_8	38
		$\pi^1_{9/2}$	ν^{-2}_6	38
3220	$23/2^+$	$\pi^1_{9/2}$	ν^{-2}_8	77
3446	$25/2^+$	$\pi^1_{9/2}$	ν^{-2}_8	82
4301	$27/2^+$	$\pi^1_{9/2}$	ν^{-4}_{10}	61
		$\pi^1_{9/2}$	ν^{-4}_9	15
4592	$29/2^+$	$\pi^1_{9/2}$	ν^{-4}_{10}	72
		$\pi^3_{13/2}$	ν^{-2}_8	14
5620	$31/2^+$	$\pi^1_{9/2}$	ν^{-4}_{12}	77
5841	$33/2^+$	$\pi^1_{9/2}$	ν^{-4}_{12}	52
6810	$35/2^+$	$\pi^3_{21/2}$	ν^{-2}_8	52
7140	$37/2^+$	$\pi^3_{21/2}$	ν^{-2}_8	70
		$\pi^3_{17/2}$	ν^{-4}_{10}	20
8062	$39/2^+$	$(\pi^2\bar{\pi}^1)_{17/2}$	$(\nu^{-3}\bar{\nu}^{-1})_{11}$	92
8432	$41/2^+$	$\pi^3_{21/2}$	ν^{-4}_{10}	72
		$\pi^3_{17/2}$	ν^{-4}_{12}	23
9997	$45/2^+$	$\pi^3_{21/2}$	ν^{-4}_{12}	100
Negative Parity				
0	$1/2^-$	$\bar{\pi}^1_{1/2}$		73
		$(\pi^2\bar{\pi}^1)_{5/2}$	ν^{-2}_2	14
200	$3/2^-$	$(\pi^2\bar{\pi}^1)_{3/2}$		40
		$\bar{\pi}^1_{1/2}$	ν^{-2}_2	39
334	$5/2^-$	$(\pi^2\bar{\pi}^1)_{5/2}$		53
		$\bar{\pi}^1_{1/2}$	ν^{-2}_2	27
840	$7/2^-$	$\bar{\pi}^1_{1/2}$	ν^{-2}_4	31
		$(\pi^2\bar{\pi}^1)_{3/2}$	ν^{-2}_2	24
		$(\pi^2\bar{\pi}^1)_{7/2}$		14
1169	$9/2^-$	$(\pi^2\bar{\pi}^1)_{9/2}$		38
		$(\pi^2\bar{\pi}^1)_{5/2}$	ν^{-2}_2	32
		$\bar{\pi}^1_{1/2}$	ν^{-2}_4	13
1604	$11/2^-$	$\bar{\pi}^1_{1/2}$	ν^{-2}_6	42
		$(\pi^2\bar{\pi}^1)_{3/2}$	ν^{-2}_4	10
1977	$13/2^-$	$(\pi^2\bar{\pi}^1)_{13/2}$		48
		$(\pi^2\bar{\pi}^1)_{9/2}$	ν^{-2}_2	20
2277	$15/2^-$	$\bar{\pi}^1_{1/2}$	ν^{-2}_8	32
		$\pi^1_{9/2}$	$(\nu^{-1}\bar{\nu}^{-1})_5$	12
2412	$17/2^-$	$(\pi^2\bar{\pi}^1)_{17/2}$		61
		$(\pi^2\bar{\pi}^1)_{17/2}$	ν^{-2}_2	18
2905	$19/2^-$	$(\pi^2\bar{\pi}^1)_{3/2}$	ν^{-2}_8	16
		$\bar{\pi}^1_{1/2}$	ν^{-4}_{10}	10
3219	$21/2^-$	$(\pi^2\bar{\pi}^1)_{17/2}$	ν^{-2}_2	26
		$(\pi^2\bar{\pi}^1)_{5/2}$	ν^{-2}_8	13
4286	$23/2^-$	$(\pi^2\bar{\pi}^1)_{7/2}$	ν^{-2}_8	8
		$(\pi^2\bar{\pi}^1)_{15/2}$	ν^{-2}_4	7
4131	$25/2^-$	$(\pi^2\bar{\pi}^1)_{17/2}$	ν^{-2}_4	37
		$(\pi^2\bar{\pi}^1)_{13/2}$	ν^{-2}_6	13
		$(\pi^2\bar{\pi}^1)_{17/2}$	ν^{-2}_6	12
5302	$27/2^-$	$(\pi^2\bar{\pi}^1)_{17/2}$	ν^{-2}_8	37
		$(\pi^2\bar{\pi}^1)_{17/2}$	ν^{-2}_6	27
		$(\pi^2\bar{\pi}^1)_{17/2}$	ν^{-4}_7	11
5010	$29/2^-$	$(\pi^2\bar{\pi}^1)_{17/2}$	ν^{-2}_6	63
		$(\pi^2\bar{\pi}^1)_{13/2}$	ν^{-2}_8	19
5592	$31/2^-$	$(\pi^2\bar{\pi}^1)_{17/2}$	ν^{-2}_8	76
		$(\pi^2\bar{\pi}^1)_{17/2}$	ν^{-4}_7	10
6039	$33/2^-$	$(\pi^2\bar{\pi}^1)_{17/2}$	ν^{-2}_8	86
		$(\pi^2\bar{\pi}^1)_{13/2}$	ν^{-4}_{10}	11
6745	$35/2^-$	$(\pi^2\bar{\pi}^1)_{17/2}$	ν^{-4}_{10}	52
		$(\pi^2\bar{\pi}^1)_{17/2}$	ν^{-4}_9	20
7226	$37/2^-$	$(\pi^2\bar{\pi}^1)_{17/2}$	ν^{-4}_{10}	81
8255	$39/2^-$	$(\pi^2\bar{\pi}^1)_{17/2}$	ν^{-4}_{12}	68
		$\pi^3_{17/2}$	$(\nu^{-3}\bar{\nu}^{-1})_{11}$	17
		$\pi^3_{21/2}$	$(\nu^{-3}\bar{\nu}^{-1})_9$	12
8536	$41/2^-$	$(\pi^2\bar{\pi}^1)_{17/2}$	ν^{-4}_{12}	94
9815	$43/2^-$	$\pi^3_{21/2}$	$(\nu^{-3}\bar{\nu}^{-1})_{11}$	100

3 Results

3.1 The nucleus ^{86}Zr

High-spin states in ^{86}Zr were investigated by Warburton *et al.* [6] and by Chowdhury, *et al.* [7]. Within the chosen truncation, the highest spins reached for positive and negative parity are 20^+, 17^- and 19^-, if we consider the partitions $[\pi^2(g_{9/2}) \otimes \nu^{-4}(g_{9/2})]$, $[\pi(g_{9/2})\pi(p_{1/2}) \otimes \nu^{-4}(g_{9/2})]$ and $[\pi^2(g_{9/2}) \otimes \nu^{-1}(p_{1/2})\nu^{-3}(g_{9/2})]$, relative to ^{88}Sr. A large number of $B(E2)$ and $B(M1)$ values of the positive-parity yrast transitions as well as several magnetic moments were measured [6,7], via the Transient Field (TF), Recoil Distance Transient Field (RDTF) and/or static hyperfine field (IMPAD) methods [11,28,29].

A comparison of the measured and calculated level scheme is presented in fig. 1. The yrast states were separated from the yrare states in order to better correlate the predicted states with their experimental partners. In particular, one notes the doubling of the positive-parity states for $I^\pi = 8^+$, 10^+, 12^+, and 14^+. The calculations reproduce the fact that the yrast band up to spin 14^+ has $E2$ character, followed by $M1$ transitions up to spin 20^+. The main discrepancy between theory and experiment is the very different level structure below spin 8^+. The shell model predicts predominantly seniority $v_\nu = 2$

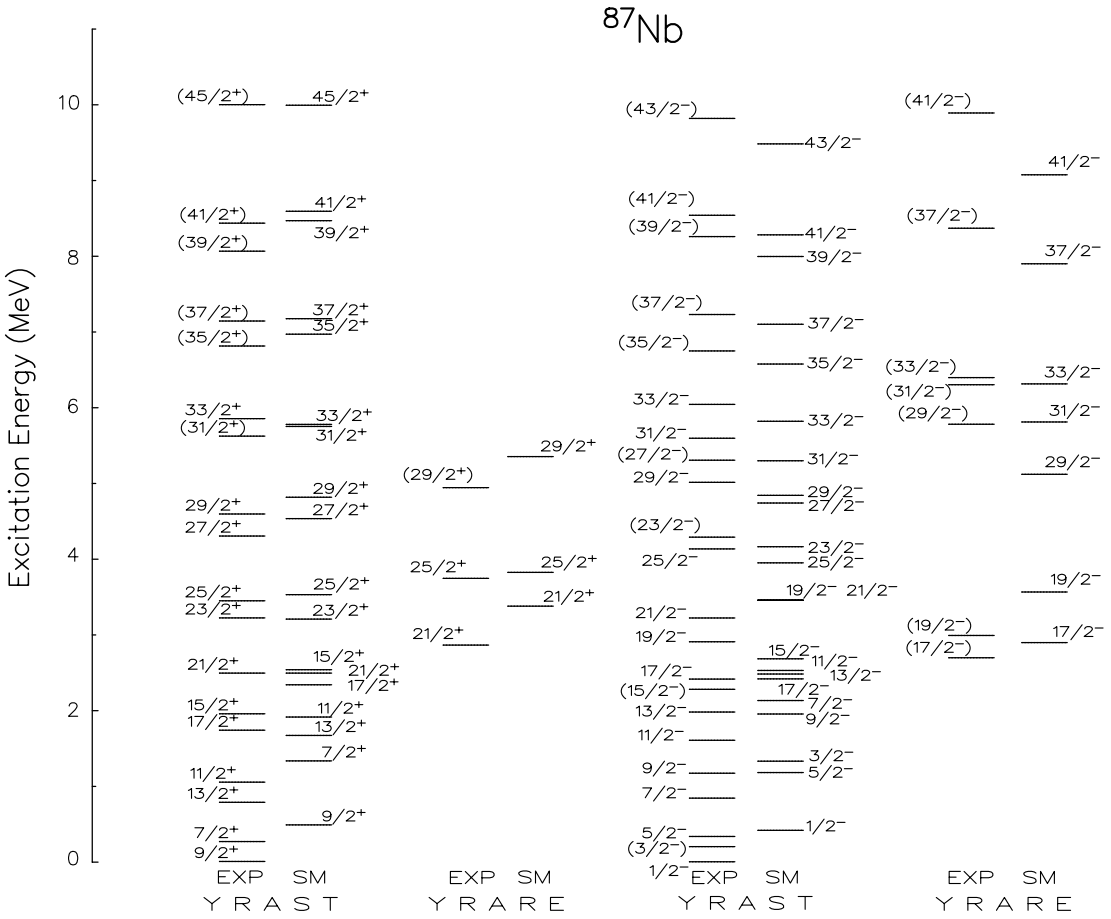

Fig. 3. Experimental [8] and theoretical high-spin level scheme in ^{87}Nb.

neutron configurations, $\nu^{-2}(g_{9/2})$, giving rise to a typical $(g_{9/2})^2$ spectrum, in contrast to the roughly equidistant experimental level spacing. On the negative-parity side, the situation is even more complex, due to the high density of predicted states in the spin range $I^\pi = 7^-$–13^- of which only the yrast levels are shown in fig. 1. Note that the close multiplet 8^-–11^- is not found experimentally. The experimental yrast sequence has $E2$ character, while the shell model gives alternative $E2$ and $M1$ transitions. The calculated leading partitions of the wave functions in ^{86}Zr are given in table 1 and a comparison of measured and calculated branching ratios is given in table 2.

As previously noted [7] and displayed in fig. 2a, the $M1$ strengths along the positive-parity yrast sequence show an alternating strength pattern in the spin range 14^+ – 20^+, with $B(M1)$ oscillating between 0.07 and 0.8 W.u. The shell model calculation reproduces this interesting feature and even overdramatizes the staggering. The underlying reason is very simple: the predicted predominant partitions of the 20^+ and 19^+ states are $[\pi^2(g_{9/2})_8 \otimes \nu^{-4}(g_{9/2})_{12}]$ and allow a strong $M1$ transition to take place by just recoupling the total proton and neutron spins, I_π and I_ν. The $19^+ \rightarrow 18^+$ $M1$ transition, on the other hand, is strongly retarded, since the main partition of the 18^+ state, $[\pi^2(g_{9/2})_8 \otimes \nu^{-4}(g_{9/2})_{10}]$, requires a recoupling of the neutron spin by $2\hbar$ which cannot proceed via the $M1$ operator. In spite of the more complex partitions of the lower-spin yrast states, the same argument holds for the full $M1$ structure. The reduction in theoretical $M1$ strengths of the favored transitions for decreasing spin, *i.e.* for the $20^+ \rightarrow 19^+$, $18^+ \rightarrow 17^+$ and $16^+ \rightarrow 15^+$ transitions, directly measures the decreasing components having mainly fully aligned proton and neutron spins, *i.e.* $[\pi^2(g_{9/2})_8 \otimes \nu^{-2,4}(g_{9/2})_{I_\nu}]$, $I_\nu = 12$, 10 or 8.

In this nucleus, Chowdhury and collaborators [7] applied an interacting boson plus n quasi-particle model (IBM-$n$qp, $n = 0$, 2 or 4) to account for the obviously more collective level structure at low spins. These authors used an IBM-1 representation of the (slightly anharmonic vibrational) core, without differentiating between protons and neutrons in the core, and by using either protons or neutrons in the qp part of the wave functions. In this approach, the total spin $I = I_c + I_{qp}$ is composed of the core spin I_c and the $n$qp spin I_{qp}. When constructing the states of high angular momenta, one has the choice between either increasing the d-boson spin I_c of the core ($I_c \leq$ twice the boson number $N_d = 7$) or the number of quasi-particle, n. The staggering of $M1$ strengths at spin 14^+ – 20^+ was qualitatively reproduced by using aligned 4qp spins (either protons or neutrons: $I_{qp} = 12$) and rel-

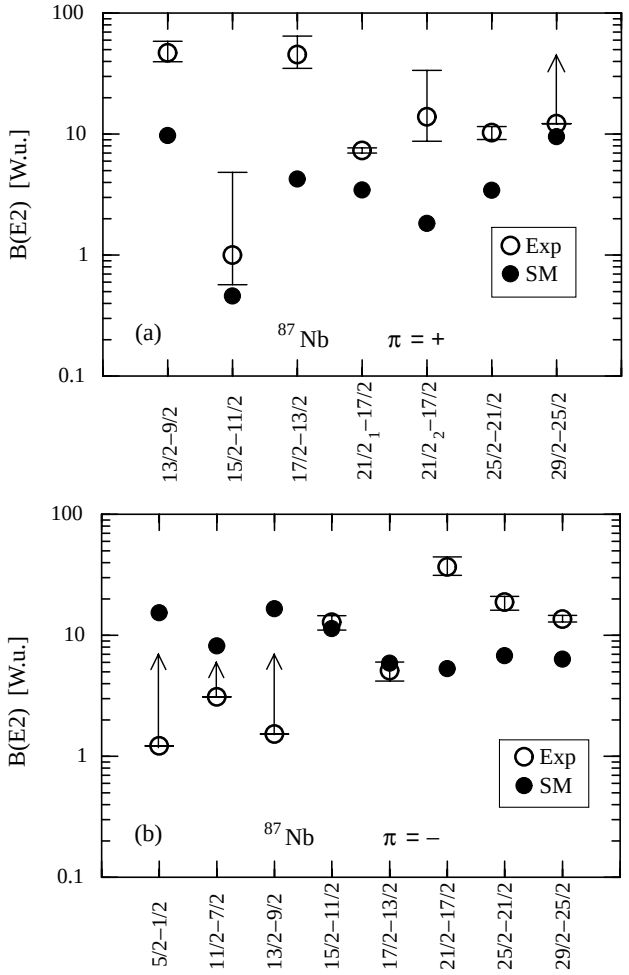

Fig. 4. Comparison of experimental [8] and theoretical $E2$ transition strengths at positive parity (a) and negative parity (b) in ^{87}Nb.

atively small values of $I_c \leq 8$ (see fig. 2a). Consequently, pairs of yrast states (20^+,19^+; 18^+,17^+; and so on) have the same quantum numbers (I_c,I_{qp}) and therefore are connected via strong $M1$ transitions within the same multiplets. For the same reason, the $M1$ transitions $19^+ \rightarrow 18^+$, $17^+ \rightarrow 16^+$ etc. vanish, due to the necessary change of the core spin I_c by $2\hbar$. In the shell model approach, the weak $M1$ strengths are a consequence of the small components of the wave functions. In conclusion, the present shell model and previous IBM-$n$qp calculations suggest that for building the high spins, more than two active nucleons have to be considered which lead to the observed pronounced staggering of $M1$ transition strengths. Furthermore, it is interesting to note that the shell model in the simple $(g_{9/2})^4$ representation already gives a good interpretation of this staggering.

In fig. 2b the experimental $E2$ strengths at positive parity are compared with the shell model predictions. One notes that the experimental $B(E2)$'s scatter between 3 and 20 W.u., with a tendency to rise to about 20 W.u. above spin 17^+. The shell model predictions are in rather good agreement with the data over the full spin range, but dramatize the minimum in $B(E2)$ for the $8^+ \rightarrow 6^+ \rightarrow 4^+$ sequence, for which theory predicts $B(E2) < 1$ W.u. Likewise, they underestimate the $B(E2)$ values of states above spin 17^+.

3.2 The nucleus ^{87}Nb

Level energies, lifetimes and magnetic moments of high-spin states in ^{87}Nb have been determined by the Göttingen group [8–12,28]. Very recently, superdeformed bands have been identified in this isotope [30], but are outside the scope of this article. Figure 3 illustrates the measured and calculated level scheme extending up to the tentative $(45/2^+)$ and $(43/2^-)$ yrast states. The levels have been ligned up at the $21/2^+$ yrast state. Experimentally, one finds, at positive parity, a stretched $E2$ band up to $21/2^+$, followed by a $M1$ structure up to $33/2^+$. On the negative-parity side, mainly stretched $M1$ and a few $E2$ yrast transitions occur. Both level sequences are well reproduced by the shell model above 2.5 MeV; similar discrepancies as in ^{86}Zr concern the level spacings of states at lower spins. With the present truncation the states between $9/2^+$ and $21/2^+$ should have mainly $[\pi(g_{9/2}) \otimes \nu^{-2}(g_{9/2})]$ partitions, but evidently are more collective. Table 3 lists the calculated leading partitions of some states.

Experimental and theoretical $B(E2)$ values are displayed in fig. 4a and b. Besides the three strong $13/2^+ \rightarrow 9/2^+$, $17/2^+ \rightarrow 13/2^+$, and $21/2^- \rightarrow 17/2^-$, quadrupole transitions having collective $B(E2) = 40 - 50$ W.u., all other $E2$ strengths are around 10 W.u., with the exception of the weak $15/2^+ \rightarrow 11/2^+$ transition, $B(E2) \approx 1$ W.u. The shell model predicts $B(E2)$-values, which are lower than the experimental ones by a factor of 3, on average, and rather small variations of $B(E2)$ for increasing spin. It reproduces the drop in $E2$ strength for the $15/2^+ \rightarrow 11/2^+$ transition, which derives from the wave functions of the two states,

$$|15/2^+\rangle = 47\%[\pi(g_{9/2}) \otimes \nu^{-2}(g_{9/2})_6] + 30\%[\pi(g_{9/2}) \otimes \nu^{-2}(g_{9/2})_4] + ... \quad (1)$$

$$|11/2^+\rangle = 65\%[\pi(g_{9/2}) \otimes \nu^{-2}(g_{9/2})_2] + 21\%[\pi(g_{9/2}) \otimes \nu^{-2}(g_{9/2})_4] + ..., \quad (2)$$

whose leading terms do not connect via an $E2$ transition (because of $\Delta I_\nu = 4$), while all other components do. Obviously, more and more precise lifetime data are required in this nucleus to better disentangle the interplay of collective and few-particle motion. With regard to the scarce lifetime data in ^{87}Nb, we have also compared the measured $M1$ and $E2$ γ-ray branching ratios with the predicted ones, as shown in table 4. This information is important in order to distinguish between the closely lying yrast and yrare states. Magnetic moments of yrast states

Table 4. Experimental and calculted branching ratios in ^{87}Nb.

E_x (keV)	I_i^π	E_γ (keV)	I_f^π	b(%) Exp	b(%) GF-1	E_x (keV)	I_i^π	E_γ (keV)	I_f^π	b(%) Exp	b(%) GF-1
Positive Parity						*Negative Parity*					
1051	$11/2_1^+$	267	$13/2_1^+$	20(3)	11	334	$5/2_1^-$	134	$3/2_1^-$	n.o.	75
		1048	$9/2_1^+$	22(7)	89			334	$1/2_1^-$	100	25
		785	$7/2_1^+$	58(6)	0	840	$7/2_1^-$	506	$5/2_1^-$	84(5)	19
		88	$13/2_2^+$	n.o.	0			640	$3/2_1^-$	<16	81
1954	$15/2_1^+$	217	$17/2_1^+$	n.o.	14	1169	$9/2_1^-$	329	$7/2_1^-$	n.o.	15
		1170	$13/2_1^+$	31(3)	12			835	$5/2_1^-$	100	85
		903	$11/2_1^+$	38(3)	1	1604	$11/2_1^-$	435	$9/2_1^-$	10	10
		992	$13/2_2^+$	31(3)	73			764	$7/2_1^-$	90	90
1737	$17/2_1^+$	953	$13/2_1^+$	100	98	1977	$13/2_1^-$	373	$11/2_1^-$	n.o.	3
		774	$13/2_2^+$	n.o.	2			808	$9/2_1^-$	100	97
2861	$21/2_2^+$	370	$21/2_1^+$	40(6)	74	2277	$15/2_1^-$	301	$13/2_1^-$	<11	2
		1124	$17/2_1^+$	60(6)	26			674	$11/2_1^-$	89(4)	98
3220	$23/2_1^+$	359	$21/2_2^+$	11(4)	8	2412	$17/2_1^-$	675	$17/2_1^+$	<6	0
		729	$21/2_1^+$	89(7)	92			458	$15/2_1^+$	32(3)	0
3446	$25/2_1^+$	226	$23/2_1^+$	56(3)	81			135	$15/2_1^-$	38(3)	89
		588	$21/2_2^+$	n.o.	0			436	$13/2_1^-$	23(3)	11
		955	$21/2_1^+$	44(3)	19	2694	$17/2_2^-$	282	$17/2_1^-$	38(8)	0
3742	$25/2_2^+$	296	$25/2_1^+$	n.o.	3			417	$15/2_1^-$	n.o.	99
		522	$23/2_1^+$	46(4)	11			717	$13/2_1^-$	62(8)	1
		881	$21/2_2^+$	39(4)	0	2737	$17/2_3^-$	43	$17/2_2^-$	n.o.	0
		1251	$21/2_1^+$	15(2)	86			325	$17/2_1^-$	100	0
3869	$25/2_3^+$	127	$25/2_2^+$	n.o.	0			460	$15/2_1^-$	n.o.	92
		423	$25/2_1^+$	100	8			760	$13/2_1^-$	n.o.	8
		649	$23/2_1^+$	n.o.	23	2905	$19/2_1^-$	211	$17/2_2^-$	n.o.	2
		1378	$21/2_2^+$	n.o.	60			493	$17/2_1^-$	26(4)	7
		1008	$21/2_1^+$	n.o.	9			169	$17/2_3^-$	25(4)	73
4592	$29/2_1^+$	291	$27/2_1^+$	19(2)	55			628	$15/2_1^-$	49(4)	18
		723	$25/2_3^+$	n.o.	1	2988	$19/2_2^-$	83	$19/2_1^-$	n.o.	0
		850	$25/2_2^+$	n.o.	0			576	$17/2_2^-$	53(13)	98
		1146	$25/2_1^+$	81(6)	44			276	$17/2_1^-$	47(8)	1
4940	$29/2_2^+$	348	$29/2_1^+$	n.o.	23			251	$17/2_3^-$	n.o.	1
		639	$27/2_1^+$	n.o.	35			711	$15/2_1^-$	n.o.	0
		1071	$25/2_3^+$	n.o.	29	3219	$21/2_1^-$	231	$19/2_2^-$	11(2)	1
		1198	$25/2_2^+$	100	2			313	$19/2_1^-$	17(2)	0
		1494	$25/2_1^+$	n.o.	11			482	$17/2_3^-$	n.o.	5
5620	$31/2_1^+$	681	$29/2_2^+$	34(3)	11			525	$17/2_2^-$	n.o.	7
		1028	$29/2_1^+$	<33	75			806	$17/2_1^-$	72(4)	87
		1319	$27/2_1^+$	>33	14	4286	$23/2_1^-$	154	$25/2_1^-$	<20	0
5841	$33/2_1^+$	221	$31/2_1^+$	<9	36			1067	$21/2_1^-$	80(10)	49
		901	$29/2_2^+$	n.o.	1			1298	$19/2_2^-$	n.o.	0
		1249	$29/2_1^+$	90(6)	63			1381	$19/2_1^-$	n.o.	51
6810	$35/2_1^+$	969	$33/2_1^+$	100	98	5777	$29/2_2^-$	185	$31/2_1^-$	n.o.	5
		1190	$31/2_1^+$	n.o.	2			767	$29/2_1^-$	n.o.	8
7140	$37/2_1^+$	329	$35/2_1^+$	31(4)	85			475	$27/2_1^-$	100	84
		1299	$33/2_1^+$	69(6)	15			1646	$25/2_1^-$	n.o.	3
7619	$37/2_2^+$	809	$35/2_1^+$	62(7)	50	5592	$31/2_1^-$	582	$29/2_1^-$	100	100
		1778	$33/2_1^+$	38(5)	28			290	$27/2_1^-$	n.o.	0
8062	$39/2_1^+$	443	$37/2_2^+$	100	43	6299	$31/2_2^-$	260	$33/2_1^-$	n.o.	1
		922	$37/2_1^+$	n.o.	57			707	$31/2_1^-$	n.o.	24
		1252	$35/2_1^+$	n.o.	0			521	$29/2_2^-$	<44	11
8432	$41/2_1^+$	370	$39/2_1^+$	61(6)	4			1289	$29/2_1^-$	n.o.	64
		813	$37/2_2^+$	n.o.	3			997	$27/2_1^-$	56(13)	0
		1293	$37/2_1^+$	39(6)	93	6039	$33/2_1^-$	447	$31/2_1^-$	62(2)	95
								262	$29/2_2^-$	n.o.	0
								1029	$29/2_1^-$	<38	5
						6393	$33/2_2^-$	354	$33/2_1^-$	n.o.	2
								94	$31/2_2^-$	n.o.	0
								801	$31/2_1^-$	100	60
								616	$29/2_2^-$	n.o.	0
								1383	$29/2_1^-$	n.o.	38
						6745	$35/2_1^-$	352	$33/2_2^-$	17(3)	29
								706	$33/2_1^-$	61(8)	47
								446	$31/2_2^-$	n.o.	0
								1152	$31/2_1^-$	22(4)	25

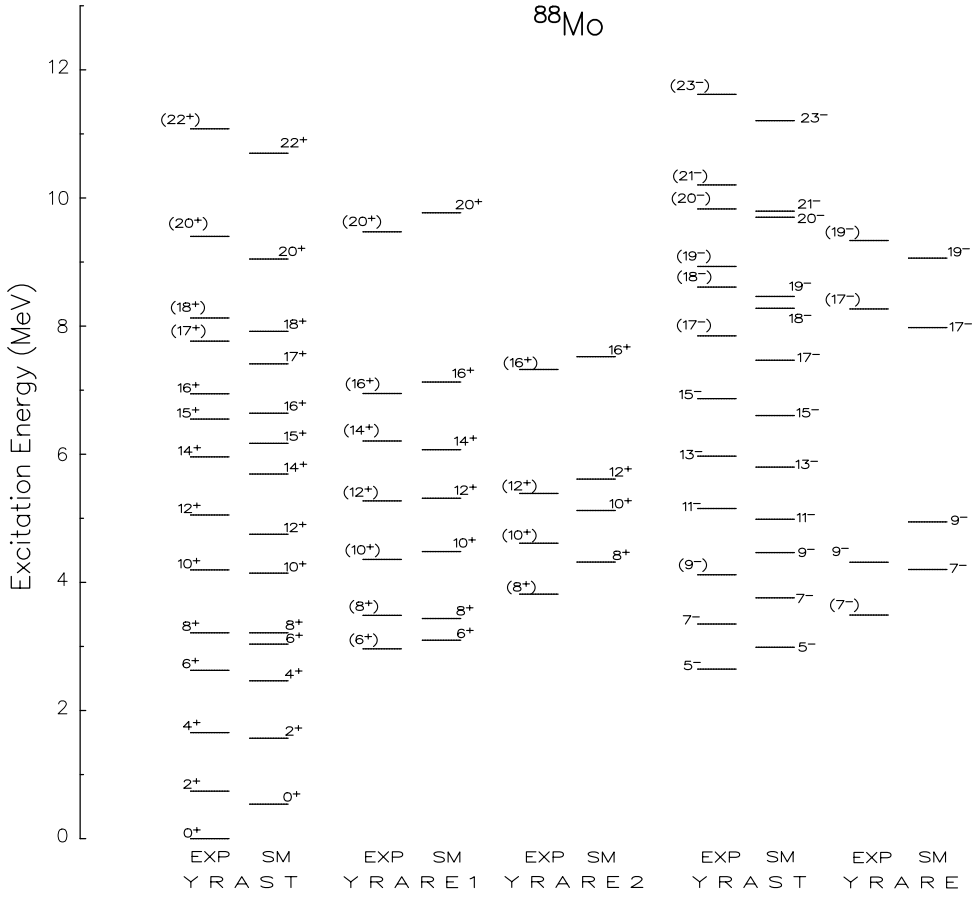

Fig. 5. Level scheme of ^{88}Mo. The data are from [12].

in ^{87}Nb have recently been determined [10,11,28]. As documented in table 5, the measured g-factors agree with the Gross-Frenkel predictions. However, the limited precision of these numbers does not allow one to distinguish between the predicted yrast and yrare configurations, which generally have very similar proton and neutron partitions, but differ by their individual spin couplings.

3.3 The nucleus ^{88}Mo

High-spin spectroscopy in this nucleus was performed by Weiszflog *et al.* [12,28] and Kabadiyski *et al.* [13]. The level scheme shown in fig. 5 has been established up to the tentative spins and parities (20_2^+) and (23^-), close to the maximum spin values of 24^+ and 23^- within the $(p_{1/2}, g_{9/2})$ model space. Similarly as in ^{86}Sr, the positive-parity yrast sequence is made up by a stretched $E2$ cascade up to 20^+, interrupted by a stretched $M1$ cascade in the interval 16^+–18^+. A similar pattern arises at negative parity. The shell model reproduces these level sequences and again predicts a large number of close-by–lying yrare states (see fig. 5).

Based on a comprehensive lifetime experiment [13], a detailed comparison of transition probabilities as given in fig. 6a-c is possible in this nucleus. At positive parity, a total of 18 $B(E2)$ values or limits are available for the comparison (see fig. 6a). The experimental $E2$ strengths cover the range from 0.5 to 40 W.u., *i.e.* nearly two orders of magnitude. Apart from very few serious discrepancies, which mainly involve yrare states, the shell model follows the experiment rather closely. For the $E2$ yrast cascade, the model predicts the strengths to slowly fall from 22 to

Table 5. Measured and calculated g-factors in ^{86}Zr and ^{87}Nb[a].

Nuclear state	E_x(keV)	I^π	Experiment[a]	Shell model
^{87}Nb	2491	$21/2^+$	+0.38(8)	+0.38
	3220	$23/2^+$	+1.36(74)	+0.31
	3446	$25/2^+$	+0.22(15)	+0.35
	4131	$25/2^-$	+0.51(39)	+0.62
	5010	$29/2^-$	+0.53(11)	+0.58
^{86}Zr	3299	8^+	−0.04(8)	−0.20
	4327	10^+	−0.58(72)	−0.09
	5397	12^+	−1.07(66)	+0.23
	6322	14^+	+2.0(4)	+0.53
	3533	8_2^+	+1.08(22)	+1.25

[a] From ref. [11].

7 W.u. in the spin range 4^+ to 14^+, while experimentally they drop from 40 to 3 W.u.

At negative parity, eight $B(E2)$ in the range 8–80 W.u. were measured (see fig. 6b). In general, the agreement is satisfactory, with the exception of the $7^- \rightarrow 5_2^-$ and $11^- \rightarrow 9_2^-$ transitions which the calculation underestimates by up to two orders of magnitude. Again, one notes that the model overemphasizes the degree of hindrance for the weak transitions, probably as a consequence of the very truncated single-particle space. In the calculation, the small $7^- \rightarrow 5_2^-$ and large $7^- \rightarrow 5_1^-$ $E2$ strengths are related to the very different partitions of the wave functions,

$$|7^-\rangle_1 = 34\%[\pi^3(g_{9/2})\pi(p_{1/2})] + 31\%[\pi(g_{9/2})\pi(p_{1/2})_5 \otimes \nu^{-2}(g_{9/2})_2] + ... \quad (3)$$

$$|5^-\rangle_1 = 57\%[\pi(g_{9/2})\pi(p_{1/2})] + 11\%[\pi(g_{9/2})\pi(p_{1/2})_4 \otimes \nu^{-2}(g_{9/2})_2] + ... \quad (4)$$

$$|5^-\rangle_2 = 54\%[\nu^{-1}(g_{9/2})\nu^{-1}(p_{1/2})] + 8\%[\pi^2(g_{9/2})_2 \otimes \nu^{-1}(g_{9/2})\nu^{-1}(p_{1/2})_4] + ... \quad (5)$$

which do forbid the $7^- \rightarrow 5_2^-$ transition and would favor the $7^- \rightarrow 5_1^-$ transition. Experimentally, both transitions are weak. Finally, fig. 6c shows a comparison of measured and calculated $M1$ strengths, which are of moderate size and, apart from the $15^+ \rightarrow 14_2^+$ transition, agree fairly well with each other. Note the retarded $14_2^+ \rightarrow 14_1^+$ and $15^+ \rightarrow 14_1^+$ $M1$ transitions which are a consequence of the main seniority $v = 4$ and 6 partitions of the states:

$$|15^-\rangle_1 = 72\%[\pi^2(g_{9/2})_8 \otimes \nu^{-2}(g_{9/2})_8] + 10\%[\pi^2(g_{9/2})_8 \otimes \nu^{-4}(g_{9/2})_7] + ... \quad (6)$$

$$|14^-\rangle_1 = 52\%[\pi^2(g_{9/2})_8 \otimes \nu^{-2}(g_{9/2})_6] + 26\%[\pi^2(g_{9/2})_6 \otimes \nu^{-2}(g_{9/2})_8] + ... \quad (7)$$

$$|14^-\rangle_2 = 45\%[\pi^2(g_{9/2})_8 \otimes \nu^{-2}(g_{9/2})_8] + 14\%[\pi^2(g_{9/2})_8 \otimes \nu^{-4}(g_{9/2})_7] + 18\%[\pi^2(g_{9/2})_6 \otimes \nu^{-2}(g_{9/2})_8] + ... \quad (8)$$

The largest components of the wave functions of the 15_1^+ and 14_1^+ states imply a vanishing $M1$ strength (since either $\Delta I_\nu = 2$ in the first component or $\Delta I_\pi = 2$ in the second component of the wave functions). Contrary to this, the $15_1^+ \rightarrow 14_2^+$ $M1$ transition would be allowed, as the partitions indicated connect via allowed $\Delta I_\pi = 0$, $\Delta I_\nu = 0$ $M1$ transitions by simple angular-momentum coupling. It is not clear why the calculation does not reproduce the measured small $M1$ strength. The retarded $15_1^+ \rightarrow 14_1^+$ $M1$ transition may have a similar origin as discussed in the case of ^{86}Zr. Lingk *et al.* [31] recently reported another striking example for such a strongly suppressed $M1$ transition: the 15^+ yrast level in ^{92}Ru decays with $B(M1; 15^+ \rightarrow 14_1^+) = 3.6$ mW.u., *e.g.*, by three orders of magnitude smaller than the favored $B(M1; 15^+ \rightarrow 14_2^+)$. In this case the shell model nicely reproduced both decay strengths.

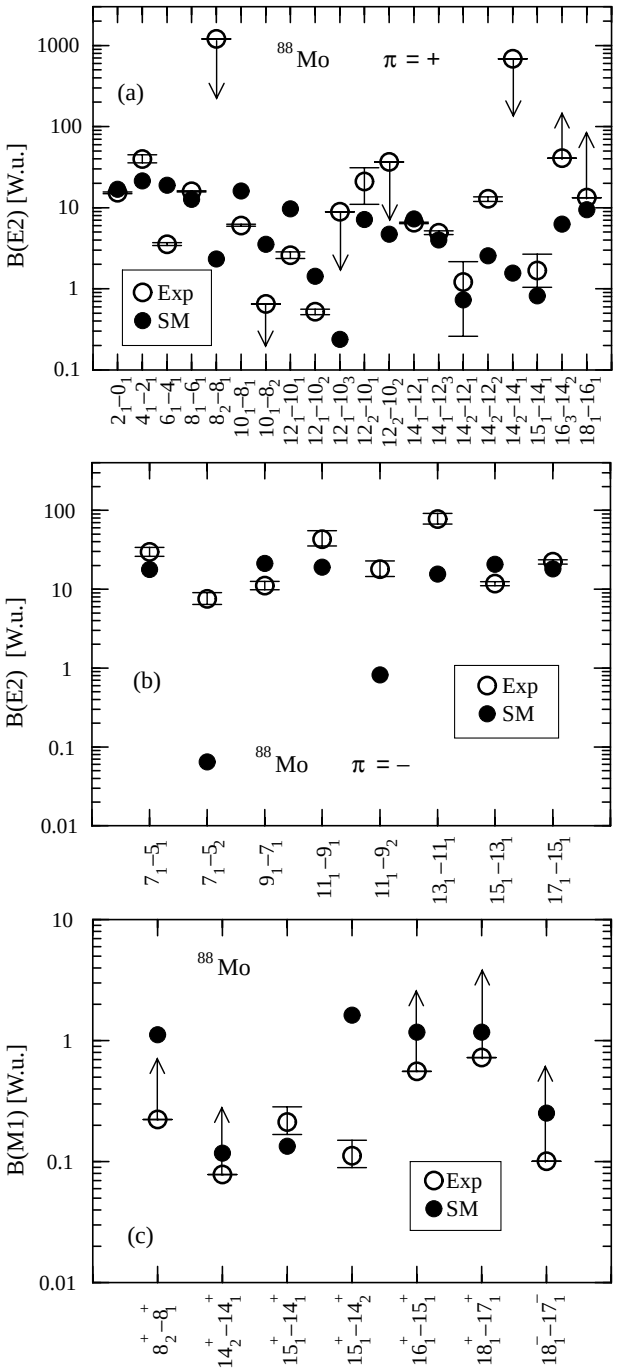

Fig. 6. Experimental [13] and shell model $M1$ and $E2$ transition strengths in ^{88}Mo: a) $E2$ strengths at positive parity; b) $E2$ strengths at negative parity; c) $M1$ strengths.

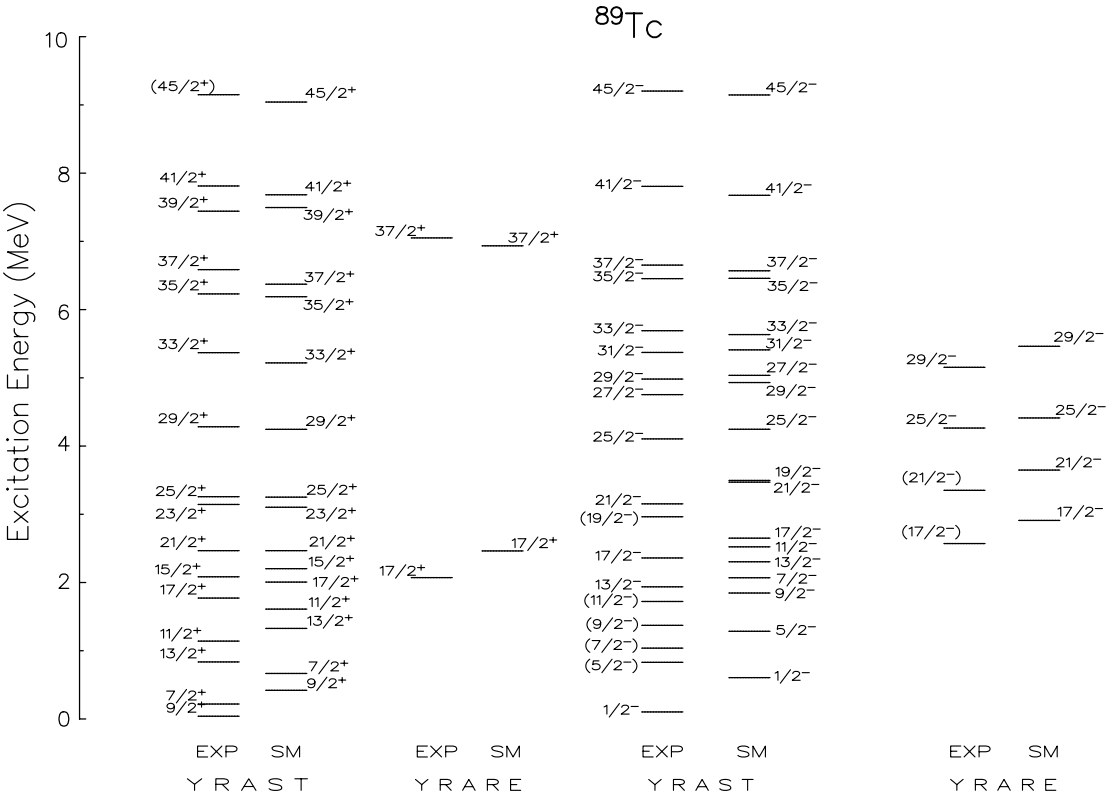

Fig. 7. Level scheme of ^{89}Tc [14,32].

3.4 The nucleus ^{89}Tc

The positive-parity yrast sequence of this nucleus was first identified by Rudolph *et al.* [14] who extended it up to the probable spin $(45/2^+)$. In addition, the negative-parity yrast band up to $45/2^-$ and several yrare states were localized. Indeed, the highest spin is $I = 49/2$, for both parities, when considering 5 protons and 4 neutron holes in the $(g_{9/2}, p_{1/2})$ model space. Apart from a few lifetime limits [15] and a detailed analysis of branching ratios [32], no measurements of electromagnetic (transition) moments are available up to now, since the cross-section for populating this nucleus is quite low.

Figure 7 compares the experimental and calculated level scheme taken from [32]. We first note that each experimental level has a closeby theoretical partner, although the calculated level scheme for both parities is systematically compressed relative to the experimental one. Rudolph *et al.* [32] pointed out that the positive-parity sequences in the two $N = 46$ isotones ^{87}Nb and ^{89}Tc are very similar and follow a simple linear correlation: $E_x(^{89}\mathrm{Tc}) = 112$ keV + 0.904 $E_x(^{87}\mathrm{Nb})$. The overall MLD = 210 keV in ^{89}Tc is again of the order of the yrast-yrare energy splitting. This may imply that some of the states are either interchanged in energy or strongly mixed. The calculated predominant partitions have been summarized in [32]. At positive parity they are $[\pi^1(g_{9/2}) \otimes \nu^{-2}(g_{9/2})]_{v=3}$ for the $13/2^+$–$25/2^+$ yrast states, $[\pi^3(g_{9/2}) \otimes \nu^{-2}(g_{9/2})]_{v=5}$ for the $29/2^+$–$37/2^+$ yrast states, and $[\pi^3(g_{9/2}) \otimes \nu^{-4}(g_{9/2})]_{v=7}$ for the $29/2_2^+$–$45/2^+$ states. At negative parity, the predicted leading components are $[\pi(p_{1/2})\pi^2(g_{9/2})]_{v=3}$ for $9/2^-$–$17/2^-$, and $[\pi(p_{1/2})\pi^2(g_{9/2}) \otimes \nu^{-2}(g_{9/2})]_{v=5}$ for $21/2^-$–$33/2^-$, respectively. In the spin range $35/2^-$–$45/2^-$, the maximum seniorities $v_\pi = 5$ and $v_\nu = 2$ or 4 are realized. Concerning the γ-ray branching ratios, we refer to the previous work [32].

3.5 The nuclei ^{90}Ru and ^{91}Rh

Positive-parity high-spin states in ^{90}Ru were identified by Heese *et al.* [16] and explained within the $(g_{9/2}, p_{1/2})$ model space. The known states and their shell model counterparts are illustrated in fig. 8, which also contains the predicted negative-parity high-spin sequence. Again the theoretical spectrum appears somewhat compressed indicating that the use of constant TBME may not be correct when moving away from the ^{88}Sr core. The positive-parity sequence has $E2$ character up to spin 12^+ and is then followed by two $M1$ and one $E2$ transitions. The states up to 8^+ are formed by mainly seniority $v = 2$ partitions and up to spin 16^+ by seniority $v = 4$ partitions. However, even at a spin as low as 4, mixing of the seniority $v = 2$ and 4 partitions $\pi^2(g_{9/2})$, $\nu^{-2}(g_{9/2})$ and $[\pi^2(g_{9/2}) \otimes \nu^{-2}(g_{9/2})]$ does occur. The states of spins $I > 8^+$, of course, require at least seniority $v = v_\pi + v_\nu = 4$. The calculations reproduce the main γ-decay path 16^+–15^+–$(14^+, 13^+)$ - 12^+–10^+,

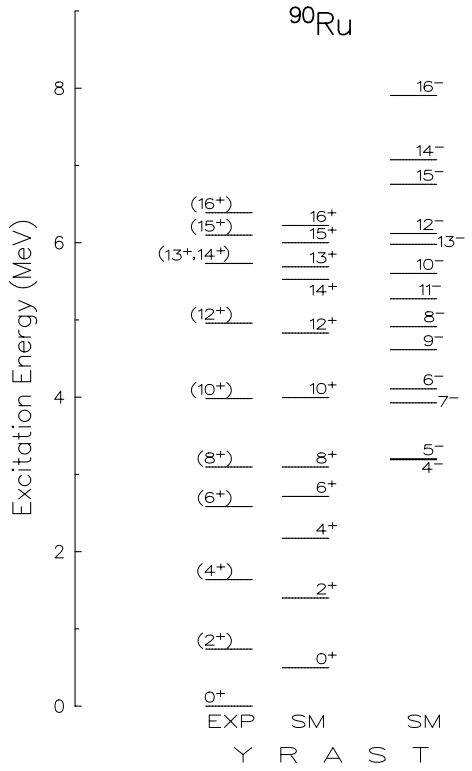

Fig. 8. Experimental and calculated level scheme of ^{90}Ru [16].

but cannot distinguish between the $I^\pi = 14^+$ and 13^+ assignments for the 5731 keV state. Neither negative-parity states nor transition strengths in this nucleus are known to us.

On the basis of the generally good agreement of the measured and predicted high-spin level schemes in the $N = 46$ isotones with proton numbers $Z = 40$–44, we also calculated the yrast spectrum of the very neutron deficient $N = 46$ isotone ^{91}Rh ($Z = 45$) which so far is not known experimentally. This spectrum is shown in fig. 9 and reaches up to $49/2^\pm$ within the $(g_{9/2}, p_{1/2})$ space. At positive parity, the calculations predict a stretched $E2$ yrast cascade up to $49/2^+$, while at negative parity the $E2$ cascade only reaches up to $17/2^-$ and is then followed by a $M1$ cascade up to $33/2^-$. The "favored" and "unfavored" stretched $E2$ transitions at both parities are predicted to have strengths of 8–24 W.u., with the exceptions of the weak $19/2^+ \rightarrow 15/2^+$, $47/2^+ \rightarrow 43/2^+$ and $19/2^- \rightarrow 15/2^-$ transitions. $M1$ transitions of the type $I \rightarrow I + 1$ should be rather strong at positive parity (0.2–1.6 W.u.) and generally stronger than that of the $I \rightarrow I - 1$ transitions.

In the neighboring isotope ^{92}Rh, Kast *et al.* [33] have recently identified yrast states up to the probable $21^\pm$ levels and found good agreement with the Gross-Frenkel shell model predictions, as proven by MLD = 103 keV at positive parity and MLD = 273 keV at negative parity. In particular, the sucession of stretched $M1$ and $E2$ transitions along the ^{92}Rh yrast cascade was reproduced in this calculation.

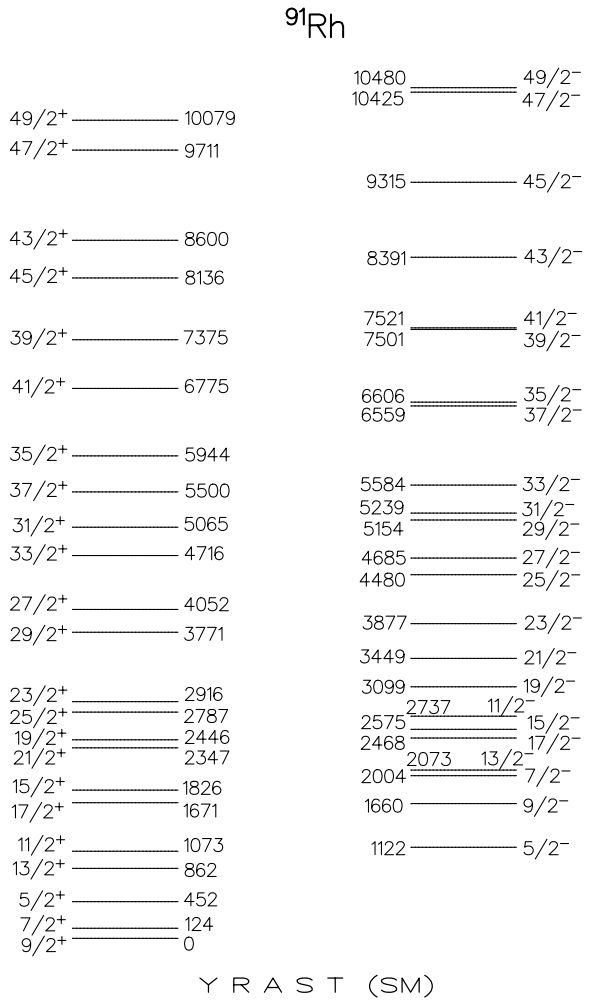

Fig. 9. Predicted yrast spectrum of ^{91}Rh.

4 Summary and conclusions

The wealth of new spectroscopic information gathered in recent years for the $N = 46$ isotones above proton number $Z = 38$ has provided the possibility to carry out detailed tests of the shell model in this transitional region. Here we have adopted the simplest approach by Gross and Frenkel within the $(g_{9/2}, p_{1/2})$ single-particle space for protons and neutrons. Different approaches have been used, *e.g.*, by Sinatkas *et al.* [34] and by Herndl and Brown [5]. The calculations by Sinatkas *et al.* [34] start from a G-matrix type realistic interaction and add two constants, besides the single-particle energies. This approach therefore has much less parameters than that using empirical interaction parameters. A survey of the positive-parity yrast spectra in the $N = 46$ isotones is documented in fig. 10. Similarities have also been established to the yrast sequences in ^{84}Sr and ^{85}Y [35,36].

The following conclusions can be drawn from the present comparison and previous work [4,5,32,37]:

1. The experimental level orderings are reproduced within a MLD of the order of 300–550 keV, if we include all states, and of 100–350 keV, if we include the states above the

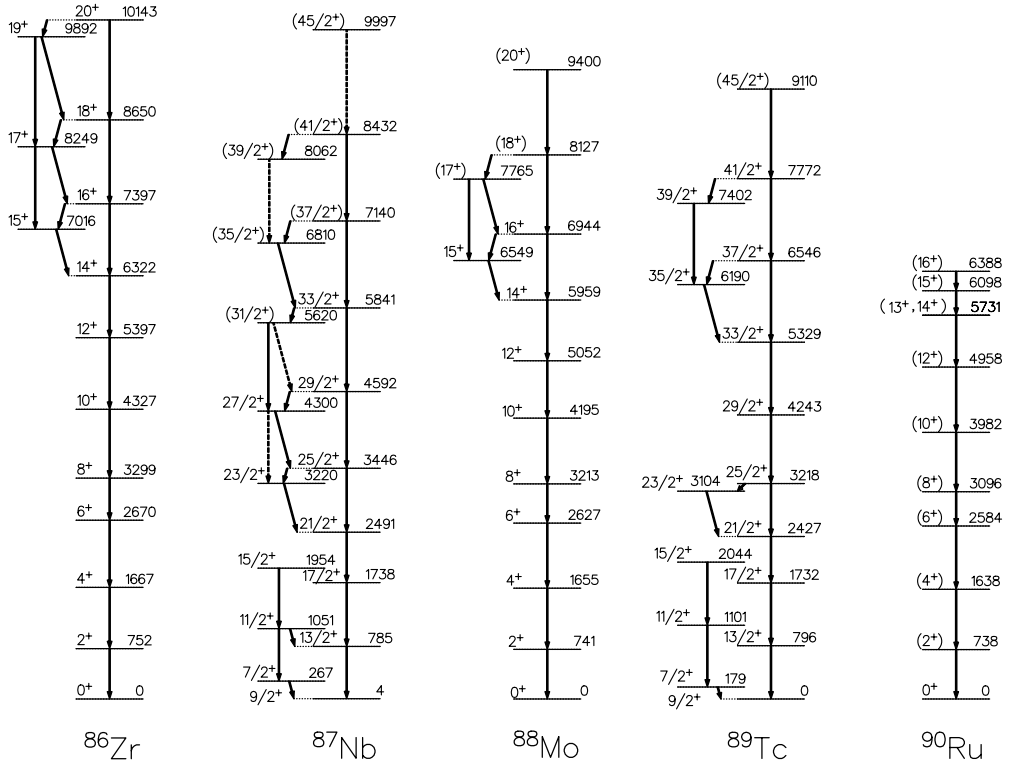

Fig. 10. Comparison of experimental positive-parity yrast bands in the $N = 46$ isotones ^{86}Zr–^{90}Ru.

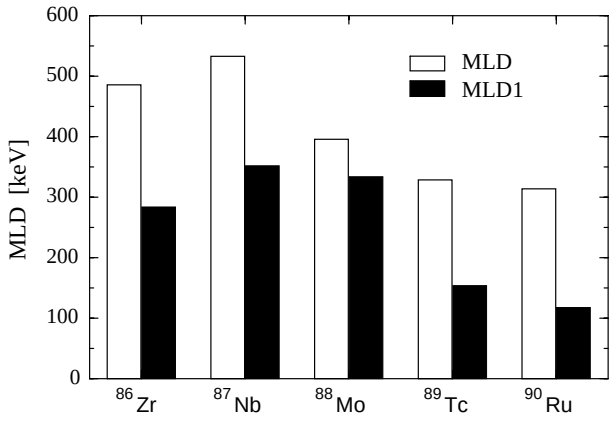

Fig. 11. Mean level deviations of $N = 46$ isotones. Open bars: all states; full bars (MLD-1): states above 8^+ (in even-even nuclei) or $21/2^+$ (in odd-A nuclei).

yrast 8^+ and $21/2^+$ levels (MLD-1, see fig. 11). These numbers are larger than for the $N = 47$–49 isotones [4], but in many cases still allow one to correlate the experimental and theoretical yrast and yrare states. At intermediate spins, several states collect sufficient γ-ray flux so that the yrast and several yrare states were identified. Theoretically, the number of closely lying states of the same spin and parity is, of course, larger than towards the termination of the structure. For both reasons, the correlation of experimental and calculated states becomes more difficult at intermediate spins and the γ-decays (as well as lifetime and magnetic moment data) are important quantities to disentangle such correlations.

2. In particular for ^{86}Zr and ^{87}Nb, the states below about 3 MeV and their $E2$ decays are not reproduced by the calculations, which generally predict too low $E2$ strengths and too large pairing effects (typical for $2j$ or $3j$ spectra, instead of the more regular level spacings shown in fig. 10).

3. Above the first alignment, the shell model structures are more clearly visible, leading to rather good agreements for both level energies and transition strengths (see the MLD-1 values displayed in fig. 11).

4. In spite of considerable mixing between components having different seniorities, several strongly retarded $M1$ transitions (*i.e.* the $M1$ staggerings in ^{86}Zr and ^{88}Mo) can be traced to good seniorities and simple spin coupling arguments. This means that there are many states consisting of completely aligned (sub)configurations and definite proton and neutron seniorities. The strong hindrance of transition strengths leads to comparatively long lifetimes of these *seniority isomers*. We recall that some of these strongly hindered decays are not reproduced by the present calculation, possibly because of the severe truncation of the single-particle space or by the lack of the model to distinguish between closely lying yrast and yrare states.

5. The measured magnetic moments in general agree with the shell model predictions, but lack precision for more stringent tests of the wave functions. In most cases, the limited experimental precision is a consequence of the short lifetimes and correspondingly small Larmor precessions of these states.

6. Besides more precise g-factor measurements, accurate lifetime data in ^{87}Nb, ^{89}Tc and ^{90}Ru are most urgently needed. For instance, the GF-1 calculations predict mean lives of $\tau = 108$ ps for the 2320 keV $17/2^-$ state in ^{89}Tc and $\tau = 43$ ps for the 3096 keV 8^+ state in ^{90}Ru, respectively [4], which states thus live long enough to be accessible to recoil distance lifetime and IMPAD g-factor experiments.

On the basis of lifetime and magnetic moment experiments in the $N = 50$ isotones ^{94}Ru and ^{95}Rh, Jungclaus *et al.* [19–21] recently discussed the role of an enlarged single-particle space relative to the severe $(g_{9/2}, p_{1/2})$ truncation chosen so here. These authors considered the excitation of either a proton $(f_{5/2}, p_{3/2}) \rightarrow (g_{9/2}, p_{1/2})$ and/or of a neutron $(g_{9/2}, p_{1/2}) \rightarrow d_{5/2}$. Both extensions of the model space were found to lead to rather well-separated "families" of the $N = 50$ states, which are connected via extremely weak $M1$ and $E2$ transitions. This kind of isomerism again results from the fact that the wave functions have good proton and neutron seniorities and usually require simultaneous spin recouplings of both protons and neutrons in the transitions. It is interesting to note that a few yrast states in the $N = 50$ isotones of $[\pi^{-1}(p_{3/2}, f_{5/2})\pi(g_{9/2}, p_{1/2})]$ structure are located in the 2.5 MeV gap separating the pure $\pi, \nu(g_{9/2}, p_{1/2})$ and the $\pi(g_{9/2}, p_{1/2}) \otimes \nu(g_{9/2}, p_{1/2}, d_{5/2})$ families.

Extensions of the single-particle basis including the $p_{3/2}$ and $f_{5/2}$ proton orbits have been proposed by several authors, *i.e.* by Winter *et al.* [38]. The same model space has also been used by Ji and Wildenthal for the description of the $N = 50$ isotones [39]. Neutron excitations across the $N = 50$ gap have been considered by Johnstone [40].

The authors acknowledge fruitful discussions with Magda Gòrska, Dirk Rudolph and Ronald Schwengner. This work has been funded by DAAD and Deutsches Ministerium für Bildung und Forschung (BMBF).

References

1. I. Talmi and I. Unna, Nucl. Phys. **19**, 225 (1960).
2. D. H. Gloeckner and F. J. D. Serduke, Nucl. Phys. A **220**, 477 (1974); F. J. D. Serduke, R. D. Lawson and D. H. Gloeckner, Nucl. Phys. A **256** (1976) 45.
3. R. Gross and A. Frenkel, Nucl. Phys. A **267**, 85 (1976).
4. D. Rudolph, K. P. Lieb and H. Grawe, Nucl. Phys. A **597**, 298 (1996).
5. H. Herndl and B. A. Brown, Nucl. Phys. A **627**, 35 (1997)
6. E. K. Warburton, et al., Phys. Rev. C **31**, 1211 (1985); D. G. Sarantites, et al., Phys. Rev. C **57**, R1 (1998).
7. P. Chowdhury, et al., Phys. Rev. Lett. **67**, 2950 (1991); C. J. Lister, P. Chowdhury and D. Vretenaer, Nucl. Phys. A **557**, 361c (1995).
8. A. Jungclaus, et al., Z. Phys. A **340**, 125 (1991).
9. D. Kast, et al., Nucl. Phys. A **587**, 202 (1995).
10. A. Jungclaus, et al., Phys. Rev. Lett. **80**, 2793 (1998).
11. C. Teich, A. Jungclaus and K. P. Lieb, Nucl. Instr. Meth. A **418** (1998). 365; C. Teich, et al., Phys. Rev. C **59**, 1943 (1999).
12. M. Weiszflog, et al., Z. Phys. A **342**, 257 (1992).
13. M. K. Kabadiyski, et al., Phys. Rev. C **50**, 110 (1994).
14. D. Rudolph, et al., Z. Phys. A **342**, 121 (1992); Nucl. Phys. A **587**, 181 (1995).
15. D. Zainea, et al., Z. Phys. A **352**, 365 (1995).
16. J. Heese, et al., Phys. Rev. C **49**, 1896 (1994).
17. S. E. Arnell, et al., Phys. Rev. C **49**, 51 (1994).
18. H. A. Roth, et al., Phys. Rev. C **50**, 1330 (1994).
19. A. Jungclaus, et al., Phys. Rev. C **60**, 014309-1 (1999).
20. A. Jungclaus, et al., Nucl. Phys. A **637**, 346 (1998).
21. A. Jungclaus, et al., Eur. Phys. J. A **6**, 29 (1999).
22. Ch. Winter, et al., Phys. Lett. B **258**, 289 (1991); Nucl. Phys. A **535**, 137 (1991).
23. P. Moeller, J. R. Nix, W. D. Myers and W. J. Swiatecki, At. Data Nucl. Data Tabl. **59**, 185 (1995).
24. C. J. Gross, et al., Phys. Rev. C **44**, R2253 (1991).
25. F. Iachello and A. Arima, *The Interacting Boson Model*, (Cambridge University Press, Cambridge, 1987).
26. D. Zwarts, Comp. Phys. Comm. **38**, 365 (1985).
27. I. P. Johnstone and I. S. Towner, Eur. Phys. J. A **2**, 263 (1998).
28. M. Weiszflog, et al., Nucl. Phys. A **584**, 133 (1995).
29. A. W. Mountford, et al., Phys. Rev. C **51**, 513 (1995) .
30. D. R. LaFosse, et al., Phys. Rev. Lett. **78**, 614 (1997).
31. C. Lingk, et al., Phys. Rev. C **56**, R2349 (1997).
32. D. Rudolph, doctoral thesis, Universität Göttingen (1995) unpublished.
33. D. Kast et al., Z. Phys. A **356**, 363 (1997).
34. J. Sinatkas, L. D. Skouras, D. Strottman and J. D. Vergados, J. Phys. G **18**, 1401 (1992).
35. C. Garcia-Bermudez, et al., Phys. Rev. C **49**, 3309 (1994); S. Chattapadhyay, et al., Phys. Rev. C **50**, 93 (1994).
36. R. Diller, et al., Z. Phys. A **321**, 659 (1985).
37. D. Rudolph, et al., Phys. Scr. T **56**, 120 (1995).
38. G. Winter, et al., Phys. Rev. C **48**, 1010 (1993).
39. X. Ji and B. H. Wildenthal, Phys. Rev. C **37**, 1256 (1988).
40. I. P. Johnstone and L. D. Skouras, Phys. Rev. C **51**, 2817 (1995).